An adventitial IL-6/MCP1 amplification loop accelerates macrophage-mediated vascular inflammation leading to aortic dissection in mice

Brian C. Tieu,[1,2] Chang Lee,[2] Hong Sun,[2] Wanda LeJeune,[2] Adrian Recinos 3rd,[2] Xiaoxi Ju,[1] Heidi Spratt,[1,3,4] Dong-Chuan Guo,[5] Dianna Milewicz,[5] Ronald G. Tilton,[2] and Allan R. Brasier[1,2,4]

[1]Department of Biochemistry and Molecular Biology, [2]Department of Internal Medicine, Division of Endocrinology, [3]Department of Preventive Medicine and Community Health, and [4]Sealy Center for Molecular Medicine, University of Texas Medical Branch, Galveston, Texas, USA. [5]Department of Internal Medicine, University of Texas Health Science Center at Houston, Houston, Texas, USA.

Vascular inflammation contributes to cardiovascular diseases such as aortic aneurysm and dissection. However, the precise inflammatory pathways involved have not been clearly defined. We have shown here that subcutaneous infusion of Ang II, a vasopressor known to promote vascular inflammation, into older C57BL/6J mice induced aortic production of the proinflammatory cytokine IL-6 and the monocyte chemoattractant MCP-1. Production of these factors occurred predominantly in the tunica adventitia, along with macrophage recruitment, adventitial expansion, and development of thoracic and suprarenal aortic dissections. In contrast, a reduced incidence of dissections was observed after Ang II infusion into mice lacking either IL-6 or the MCP-1 receptor CCR2. Further analysis revealed that Ang II induced $CCR2^{+}CD14^{hi}CD11b^{hi}F4/80^{-}$ macrophage accumulation selectively in aortic dissections and not in aortas from *Il6*$^{-/-}$ mice. Adoptive transfer of *Ccr2*$^{+/+}$ monocytes into *Ccr2*$^{-/-}$ mice resulted in selective monocyte uptake into the ascending and suprarenal aorta in regions of enhanced ROS stress, with restoration of IL-6 secretion and increased incidence of dissection. In vitro, coculture of monocytes and aortic adventitial fibroblasts produced MCP-1– and IL-6–enriched conditioned medium that promoted differentiation of monocytes into macrophages, induced CD14 and CD11b upregulation, and induced MCP-1 and MMP-9 expression. These results suggest that leukocyte-fibroblast interactions in the aortic adventitia potentiate IL-6 production, inducing local monocyte recruitment and activation, thereby promoting MCP-1 secretion, vascular inflammation, ECM remodeling, and aortic destabilization.

Introduction

Aneurysms and aortic dissections are major diseases affecting the aorta, accounting for almost 16,000 deaths in the United States annually. Aortic aneurysms, including both abdominal and thoracic aneurysms, are highly common conditions, with abdominal aneurysms being 3 times more prevalent than thoracic aneurysms (1, 2). Although they are typically regarded as being distinct entities, vascular inflammation is a common pathogenic factor in both (3, 4). Common pathologic features of aneurysmal disease include leukocytic infiltration and structural ECM remodeling (2, 5–7). This process of aortic remodeling produces dilatation and, in some cases, acute aortic dissection or rupture, wherein the integrity of the tunica media is breached, a process resulting in high morbidity and mortality.

Vascular inflammation is a complex process involving margination, extravasation, and local activation of circulating mononuclear leukocytes into the vessel wall (8). This multistep process is the result of local secretion of chemotactic factors, macrophage-activating cytokines, upregulation of vascular adhesion molecules, and production of MMPs. Previous work has shown that MCP-1, a monocyte chemotactic factor that signals via the CCR2 receptor, is critical for aneurysm formation because of its ability to recruit leukocytes that, in turn, produce ECM-degrading MMPs, thereby inducing aortic remodeling and dilatation (9–12). However, the processes by which MCP-1 is induced in vascular inflammation have not been completely elucidated.

Of the vascular cytokines, IL-6 is well known to be secreted at high levels in human aortic aneurysm disease (13–20), has been identified as an independent biomarker of severe coronary artery disease (21–23), and is associated with risk for aneurysm rupture (13–15, 17, 19). Although IL-6 is known to induce systemic production of hepatic acute-phase reactants and facilitate survival of lymphocyte subpopulations (24, 25), its local role in aneurysm formation and exacerbation of vascular inflammatory diseases has not been clearly defined.

Cellular infiltrates of macrophages, T lymphocytes, and B lymphocytes, representing the major cell types present in human aneurysmal tissue, are mainly seen in the tunica adventitia (2, 26, 27). Besides leukocyte infiltration and cytokine production, the adventitia is highly reactive to the process of aneurysm formation, where marked proliferation, fibrosis, and myofibroblast transformation are seen (28). It is increasingly being accepted that adventitial inflammation may play a key role in the genesis and maintenance of vascular inflammation in aortic aneurysms (26, 29) and atherosclerotic vascular disease (30–33). Consequently, understanding the processes controlling cellular recruitment and leukocytic activation in the adventitia may provide fundamental insights into the pathogenesis of a diverse spectrum of cardiovascular diseases.

Conflict of interest: The authors have declared that no conflict of interest exists.
Citation for this article: *J. Clin. Invest.* **119**:3637–3651 (2009). doi:10.1172/JCI38308.

In this study, we explored mechanisms upregulating IL-6 in the aorta and how local IL-6 production contributes to vascular inflammation leading to aneurysm and dissection. We focused on macrophages, since they have a critical role in aneurysm formation (34, 35). Based on knowledge that the potent vasopressor Ang II is a strong inducer of vascular inflammation (25, 36) and aortic remodeling in atherosclerosis-prone mice (37, 38), we adapted an acute Ang II infusion model using older C57BL/6 mice, which exhibit enhanced cytokine expression compared with younger mice. Subcutaneous Ang II infusion produced aortic remodeling and aneurysm formation, with acute thoracic and abdominal aortic dissections associated with local secretion of IL-6 and MCP-1 and increased macrophage recruitment. We found that $CCR2^+$ monocytes and macrophages control the potentiation of cytokines and incidence of aortic dissection and that IL-6 promotes aortic macrophage differentiation into a pathogenic type. Moreover, we demonstrated in vitro that a cell-cell interaction between monocytes and aortic adventitial fibroblasts (AoAFs) produces similar results, leading us to suggest that it contributes significantly to the observations in vivo. In this report, we also reveal an IL-6–MCP-1 amplification loop accelerating vascular inflammation.

Results

Ang II infusion induced aortic dissection and cytokine secretion. We evaluated effects of short-term Ang II infusion into 7- to 12-month-old C57BL/6 mice at a dose of 2,500 ng/kg/min. Ang II infusion, at these doses, produces modest pressor effects; for example mean intra-arterial blood pressure after 7 days infusion was 145 ± 13 mmHg versus 109 ± 8 mmHg ($n = 3$, $P < 0.02$, 2-tailed t test; because of potential confounding effects of intravascular cannulation on hemodynamics and vascular inflammation, blood pressure was not systematically measured in this study). We observed that Ang II–treated mice developed features of aortic remodeling over 6–10 days, including aortic dilatation as previously demonstrated (37, 39) and areas of focal hemorrhages, indicating aortic dissection (Figure 1, A and B). Aortic hematomas/dissections could be demonstrated after intraventricular PBS perfusion to remove lumenal blood cells and were observed in 35% (8 of 23) of the experimental mice, with none being observed in sham-infused control mice. Dissections commonly spanned the length of the aorta from the ascending to suprarenal aorta (Figure 1B) or were located in either of 2 places, the suprarenal abdominal aorta or the ascending aorta, with the former more frequent than the latter. Analysis of aortic cross sections in the suprarenal abdominal region clearly show Ang II–induced medial hypertrophy, adventitial thickening, and blood-filled false lumens located in the tunica adventitia (Figure 1B). Moreover, clear dissections through the tunica intima and tunica media were observed in areas of hemorrhage in the ascending and suprarenal aorta (see below).

To establish the vascular cytokine response to Ang II infusion, aortic explants from young (<2 months old) and older (7–10 months of age) mice after 10 days infusion were prepared and cytokine secretion analyzed (29). Analysis of IL-6 secreted by the total aorta revealed a 3.7-fold increase in production in the young mice and a greater, 6.3-fold increase in the older mice ($P < 0.001$, 2-way ANOVA; Figure 1C). To exclude the potential underestimation of aortic cytokine production due to differences in cellular composition (vascular hemorrhage or adventitial thickening), the data were also analyzed as a function of aortic dry weight. The results were similar, with enhanced IL-6 secretion observed in the older animals (Figure 1C). Importantly, cytokine secretion was apparently independent of the presence of vascular hemorrhage; in fact, we previously have shown that cytokines are produced and secreted locally using in situ hybridization and time series analysis of aortic explants (29, 39, 40). Similarly, Ang II induced a significant, 2-fold increase in MCP-1 secretion in young animals and an enhanced, 4.7-fold increase in the older animals (Figure 1C). These changes were also significant when normalizing to aortic dry weight. The highly significant interaction term identified in all of the 2-way ANOVA analyses (IL-6, $P < 0.013$, and MCP-1, $P < 0.008$) indicates that Ang II–induced vascular cytokine production was significantly enhanced by age. To control for these age effects and enhance our ability to discern the roles of these vascular monokines, we performed all subsequent studies in older mice.

Time series analysis of monokine production in older mice showed similar responses as early as 6 days (Supplemental Figure 1; supplemental material available online with this article; doi:10.1172/JCI38308DS1), indicating that monokine production was an early event, preceding the peak in aortic dissection and aneurysm formation. Immunostaining of aortic cross sections from the ascending aorta demonstrated that IL-6 and MCP-1 were predominantly localized to the adventitia and media-adventitia border, respectively, of treated animals, with lesser staining in the intima (Figure 1D). This finding is consistent with our previous work showing that the adventitia secretes a greater amount of IL-6 per mg of tissue (29). Macrophages were detected predominantly in the adventitia along with adventitial fibroblasts (Figure 1D). Together, these data indicate that Ang II is a potent inducer of thoracic and abdominal aneurysms and dissections as well as local, adventitial vascular inflammation in this non-hyperlipidemic model.

Ang II–induced recruitment and expression of distinct activated macrophage phenotypes. Macrophages are thought to play a major role in vascular inflammation, but previous studies have only detected them in aortic tissue with generic mouse macrophage markers and semiquantified their recruitment by immunohistochemistry (IHC). Although these studies have been valuable, IHC methods are subject to significant sampling bias due to regional differences in macrophage recruitment. To remove the sampling bias and facilitate systematic analysis of activated subsets of aortic macrophages, we adapted a collagenase/elastase digestion method to dissociate the cellular aortic components for quantitative, multiparametric flow cytometry analysis. Under these conditions of dissociation, nearly complete dissolution of the aorta was observed, indicated by the reduction in the mass of residual aortic tissue and loss of intracellular β-actin staining (Supplemental Figures 2 and 3). To further characterize the aortic components, we examined dissociated cells by H&E staining. Under these conditions, well-defined planar cells were primarily identified showing characteristic eosinophilic cytoplasm and basophilic nuclear staining (Figure 2A). To specifically isolate monocytes within the dissociated aortic cell population, we subjected them to flow cytometric analysis, gating by CD14 expression. CD14 staining isolates the leukocyte population, excluding endothelial cells, smooth muscle cells, and adventitial fibroblasts (Figure 2B). To more specifically identify macrophages, the $CD14^+$ leukocytes were then gated based on CD11b expression, producing 2 distinct populations, $CD14^+CD11b^+$ and $CD14^+CD11b^-$ cells. To determine whether these populations could be considered macrophages, a third staining was performed based on F4/80 expression, a general marker for mature macrophages (41–43). It can be seen that the $CD14^+CD11b^+$ cells stained

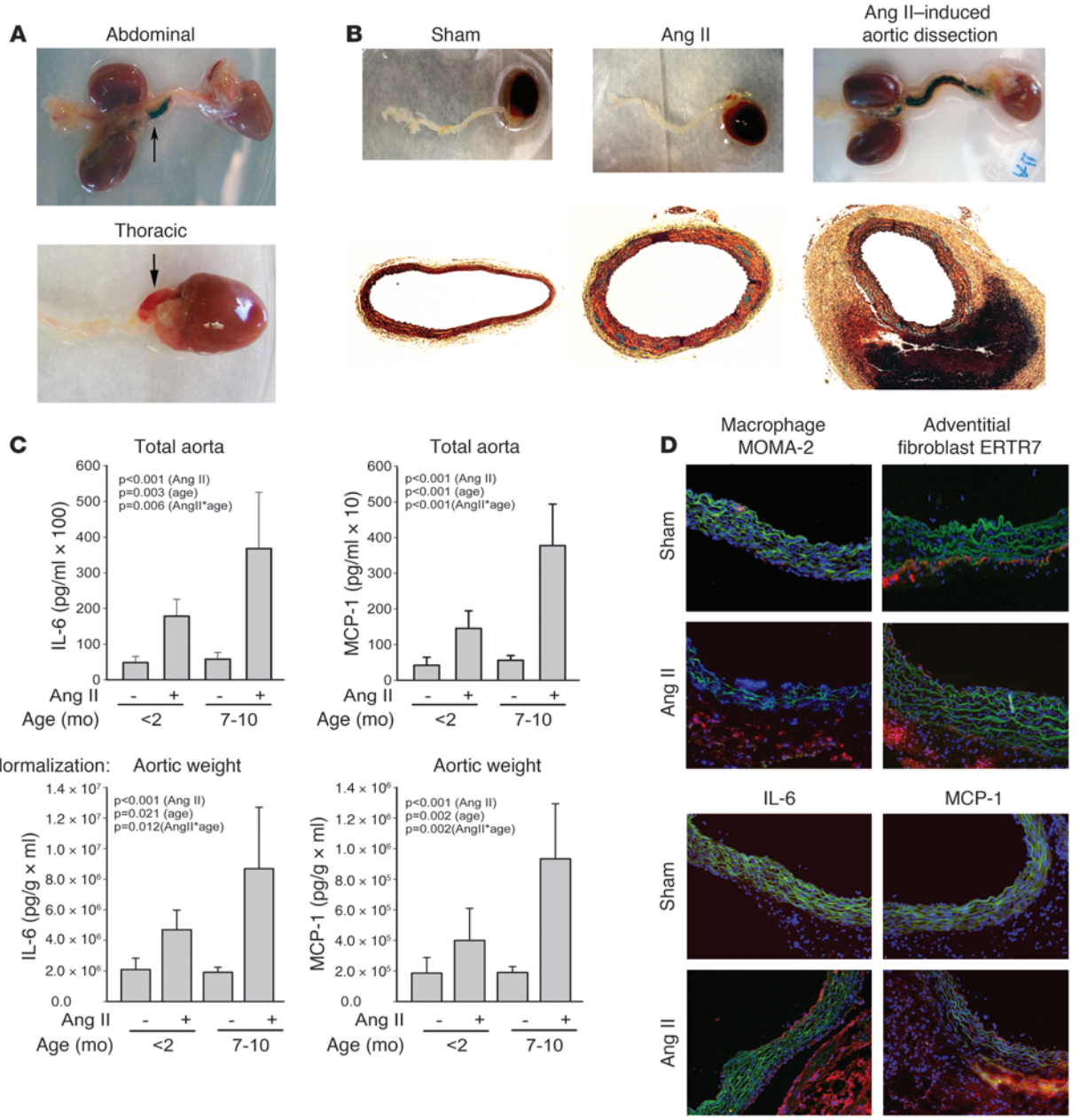

Figure 1

Ang II infusion in older WT mice induces aortic cytokines and dissecting aortic aneurysms. (**A**) Development of suprarenal abdominal and thoracic aortic dissections; dissected aortae were photographed oriented with the kidney to the left and heart to the right. (**B**) Photographs of sham- and Ang II–treated groups (top) and Movat staining of their cross sections (bottom). Original magnification, ×40. See Supplemental Figure 5 for enlarged photograph. (**C**) Secreted IL-6 and MCP-1 concentrations in aortic explant culture from sham- (n = 8) or Ang II–infused mice after 10 days (n = 12) for mice younger than 2 months of age or 7–10 months of age. Top panels show measurements after incubation of the entire aorta; bottom panels show cytokine concentrations in explant media normalized to aortic dry weight. Data are mean ± SEM. Groups were compared by 2-way ANOVA, using treatment (Ang II) or age as independent variables. For each comparison, the P value is displayed for age effect, Ang II effect, and the interaction effect of Ang II with age (AngII*age). (**D**) Immunofluorescence staining for macrophages (MOMA-2), AoAFs (ERTR7), IL-6, and MCP-1 in transverse cryosections (6 μm) of ascending aorta from sham- and Ang II–treated mice for 6 days. Nuclei were stained with DAPI (blue). Elastic lamellae of the media are green (autofluorescence). Positive staining is red (Alexa Fluor 568–conjugated secondary Ab). Original magnification, ×200.

with F4/80, while the $CD14^+CD11b^-$ cells did not. Therefore, we concluded that aortic macrophages are $CD14^+CD11b^+$ in control conditions. Backgating was performed on that population to determine the location of macrophages in a forward- versus side scatter (FSC-H versus SSC-A) dot plot, which was used consistently as the gate to visualize macrophages in subsequent experiments. Separate control experiments showed that approximately 87% of the cells contained in this gate were viable, as assessed by exclusion

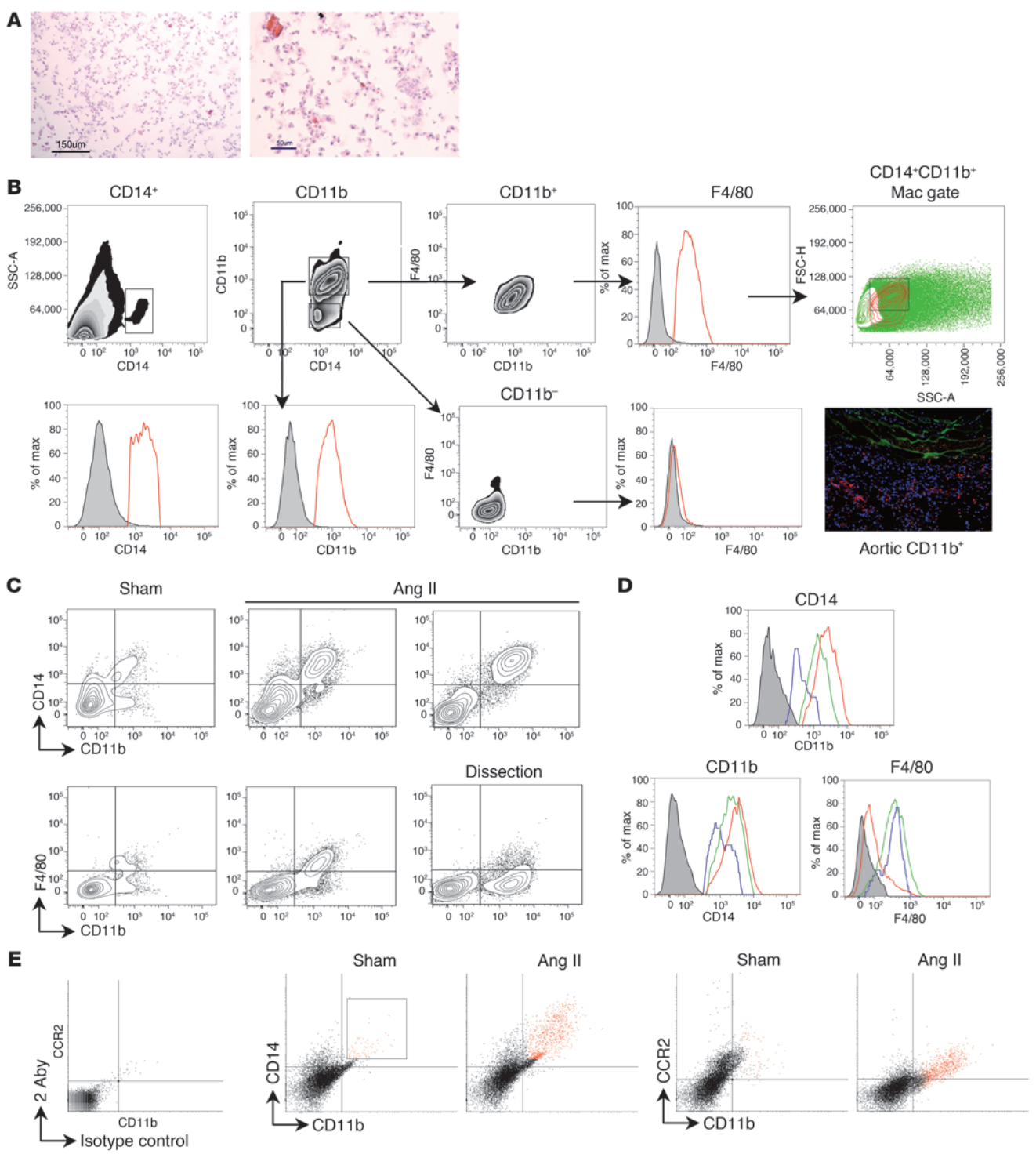

Figure 2

Aortic macrophages in WT mice display different phenotypes in response to Ang II. (**A**) Cytospin preparation of dissociated aortic tissue stained with H&E. Scale bars: 150 μm (left), 50 μm (right) (original magnification: ×200 [left]; ×400 [right]). (**B**) Dissociated aortic cells were gated on CD14 (top left); histogram with isotype control (gray) is shown at bottom left. $CD14^+$ cells were separated into $CD14^+CD11b^+$ and $CD14^+CD11b^-$ cells. $CD11b^+$ cells were confirmed by histogram as compared with isotype control. $CD14^+CD11b^+$ cells were $F4/80^+$, while $CD14^+CD11b^-$ cells were $F4/80^-$. $CD14^+CD11b^+F4/80^+$ were backgated to reveal the macrophage population (red contour circles, top right). Immunofluorescence staining for macrophages ($CD11b^+$) shows adventitial localization. Original magnification, ×200. (**C**) $CD14^+CD11b^+F4/80^+$ macrophages present in sham-treated aortas of WT mice are recruited by Ang II treatment. Macrophages in aortic dissections are increased in number but lack F4/80. (**D**) Histograms comparing expression of CD14, CD11b, and F4/80 on macrophage populations in sham-infused aortas (blue curve), Ang II–infused aortas (green curve), and Ang II–infused aortas with aortic dissection (red curve). (**E**) Ang II recruits $CCR2^+$ macrophages. Far left: Secondary Ab (2 Aby). Middle panels: $CD14^+CD11b^+$ macrophages were gated in sham- and Ang II–infused aortas and identified as $CCR2^+CD11b^+$ (red, right panels).

Table 1
Quantitation of aortic macrophages in the aorta

Genotype	Treatment	No. macrophages	% Macrophages	*n*
C57BL/6J	Sham	1,840 ± 314	0.46 ± 0.08	15
C57BL/6J	Ang II, no dissection	9,750 ± 2,218	2.44 ± 0.55	11
C57BL/6J	Ang II, dissection	127,452 ± 9.575	31.87 ± 2.39	4
Il6$^{-/-}$	Sham	1,317 ± 217	0.33 ± 0.05	9
Il6$^{-/-}$	Ang II	4,812 ± 998	1.20 ± 0.25	8
Ccr2$^{-/-}$	Sham	942 ± 102	0.24 ± 0.03	7
Ccr2$^{-/-}$	Ang II	2,626 ± 106	0.66 ± 0.03	7

Numbers of CD14^{+}CD11b^{+} macrophages in sham-treated and Ang II–treated WT, *Il6*$^{-/-}$, and *Ccr2*$^{-/-}$ mice were quantitated by flow cytometry after 6 days of Ang II infusion and expressed as a percentage of all cells counted. Data are mean ± SEM.

of ethidium homodimer (Supplemental Figure 4). In this population, a population of CD11b^{+} cells was detected; this finding combined with the immunofluorescence staining results showing that CD11b^{+} cells were predominantly localized in the adventitia lead us to suggest that the macrophage population is largely recruited into the adventitial layer of Ang II–treated mice. This finding is similar to the results of MOMA-2 staining (Figure 1).

We next analyzed the effects of Ang II infusion on macrophage populations and found a 5.3-fold increase in the number of CD14^{+}CD11b^{+} aortic macrophages (Figure 2C). In aortas with dissection, the number was even higher, with macrophages constituting 32% of all cells in aortas with dissection, while control aortas had less than 1% macrophages (Table 1). We also observed that the expression of CD14 and CD11b increased with treatment and was highest on macrophages from dissected aortas (Figure 2C). While these macrophages appeared as a distinct population separate from the other 2 groups, the most striking finding was that these macrophages were F4/80^{-}. The loss of F4/80 has been reported to occur in activated macrophages (41–43). Histograms comparing the expression of CD14, CD11b, and F4/80 in each group are shown in Figure 2D. Aortic macrophages in treated mice also expressed CCR2 (Figure 2E; specificity controls are in Supplemental Figure 6). Together, these data indicate that Ang II induces recruitment and activation of macrophages into the aortae and that a separate activated macrophage population is seen in those with acute dissections.

Role of local CCR2 signaling in vascular inflammation and formation of aortic dissections. Since recruited aortic macrophages in Ang II–treated C57BL/6J WT mice express the MCP-1 receptor CCR2, we explored the role of MCP-1 signaling on macrophage recruitment and vascular inflammation. We found that CCR2 deficiency significantly reduced Ang II–induced aortic dissections. Both sham- and Ang II–infused mice had greatly reduced numbers of aortic macrophages, and only a 2.8-fold increase was observed with Ang II infusion (Table 1). Staining for CD14^{+}CD11b^{+} aortic macrophages in treated and control *Ccr2*$^{-/-}$ mice is shown in Figure 3A. Upon analysis of conditioned medium from aortic explants, secreted IL-6 levels increased significantly between Ang II– and sham-treated groups, but by only 2.0-fold ($P < 0.03$), and MCP-1 showed a trend to be higher in treated versus sham mice, but this difference did not reach significance ($P < 0.089$; Figure 3B). These levels also were appreciably lower than the levels observed in treated WT mice after 6 days of infusion (3.6-fold for IL-6 and 6.5-fold for MCP-1; Supplemental Figure 1). These data indicated that CCR2 signaling is important in Ang II–induced vascular inflammation.

To determine whether CCR2 signaling in recruited macrophages mediated the increase in cytokines and aortic dissections, we performed adoptive transfer of *Ccr2*$^{+/+}$ (WT) monocytes into the *Ccr2*$^{-/-}$ background. Isolated isogenic *Ccr2*$^{+/+}$ or *Ccr2*$^{-/-}$ monocytes were purified, double labeled with separately detectable DiR800 and PKH26 vital dyes, and injected into tail veins of *Ccr2*$^{-/-}$ recipients pretreated with saline (sham) or Ang II (6 days). Recipients were imaged for monocyte uptake and aortic remodeling 4 days later. DiR800 was used to track the monocytes using near-infrared imaging, which assigned a green color to the monocytes (Figure 3C). Here, labeled monocytes were detected in the spleen on dorsal view and in the liver on ventral view in both sham- and Ang II–infused mice with equal intensity, implying equivalent transfer. This was confirmed by imaging the abdominal contents ex vivo (Figure 3C).

We found that *Ccr2*$^{+/+}$ monocytes injected into sham mice and *Ccr2*$^{-/-}$ monocytes injected into either sham- or Ang II–treated mice homed to the infrarenal aorta. Interestingly, Ang II treatment produced 2 regions of enhanced *Ccr2*$^{+/+}$ monocyte recruitment that coincided with regions of aortic dilatation and dissection (Figure 3D). Specifically, *Ccr2*$^{+/+}$ monocyte homing occurred exclusively in the aortic root/ascending aorta (5 of 7 mice, compared with sham treatment, 0 of 6 mice; $P < 0.03$) and the suprarenal abdominal aorta (6 of 7 mice, compared with sham treatment, 0 of 6 mice; $P < 0.01$, Fisher's exact test, 1-sided). We note the increased homing of *Ccr2*$^{+/+}$ monocytes is an independent validation of the data in Figure 2E.

Ang II induces localized vascular ROS formation. To determine whether these focal regions of macrophage recruitment corresponded to regions of enhanced ROS formation, we performed in situ dihydroethidium (DHE) staining for ROS formation. DHE is a cell-permeable dye that is oxidized by superoxide to ethidium bromide and subsequently intercalates with DNA, labeling the nuclei. In this experiment, aortas from sham- or Ang II–infused mice were separated into ascending, descending, suprarenal, and infrarenal segments and assayed for ROS formation. Strong ethidium bromide production was seen in the regions corresponding to the ascending and suprarenal aorta, corresponding to the regions of enhance recruitment of *Ccr2*$^{+/+}$ macrophages but not descending or infrarenal segments (Figure 3E and data not shown). Together, these data indicate that focal regions of macrophage recruitment overlap with regions of enhanced ROS formation.

Ccr2$^{+/+}$ *monocytes enhance vascular inflammation.* Measurement of secreted IL-6 and MCP-1 from the aortic explants of sham-treated and Ang II–treated *Ccr2*$^{-/-}$ mice receiving *Ccr2*$^{+/+}$ monocytes showed 3.7- and 9.1-fold increases, respectively (Figure 3F). In contrast, IL-6 and MCP-1 from aortic explants of sham- and Ang II–treated *Ccr2*$^{-/-}$ animals receiving *Ccr2*$^{-/-}$ monocytes showed only 2.1- and 1.9-fold increases, respectively. Two-way ANOVA analysis of these data revealed a significant interaction term ($P = 0.03$), indicating that the level of Ang II–induced MCP-1 was significantly influenced by the *Ccr2*$^{+/+}$ genotype. By contrast, analysis of IL-6 secretion indicated that only Ang II treatment had a significant effect ($P = 0.001$), without an independent or interacting role of the monocyte genotype. The level of IL-6, 26.2 ng/ml, was similar to that seen in Ang II–infused WT mice, 28.8 ng/ml, while the level of MCP-1 was greater at 2.9 ng/ml than the 1.9 ng/ml seen in treated WT mice (Figure 3F and Supplemental Figure 1). As a measure of specificity, *Ccr2*$^{+/+}$ monocyte injection did not increase

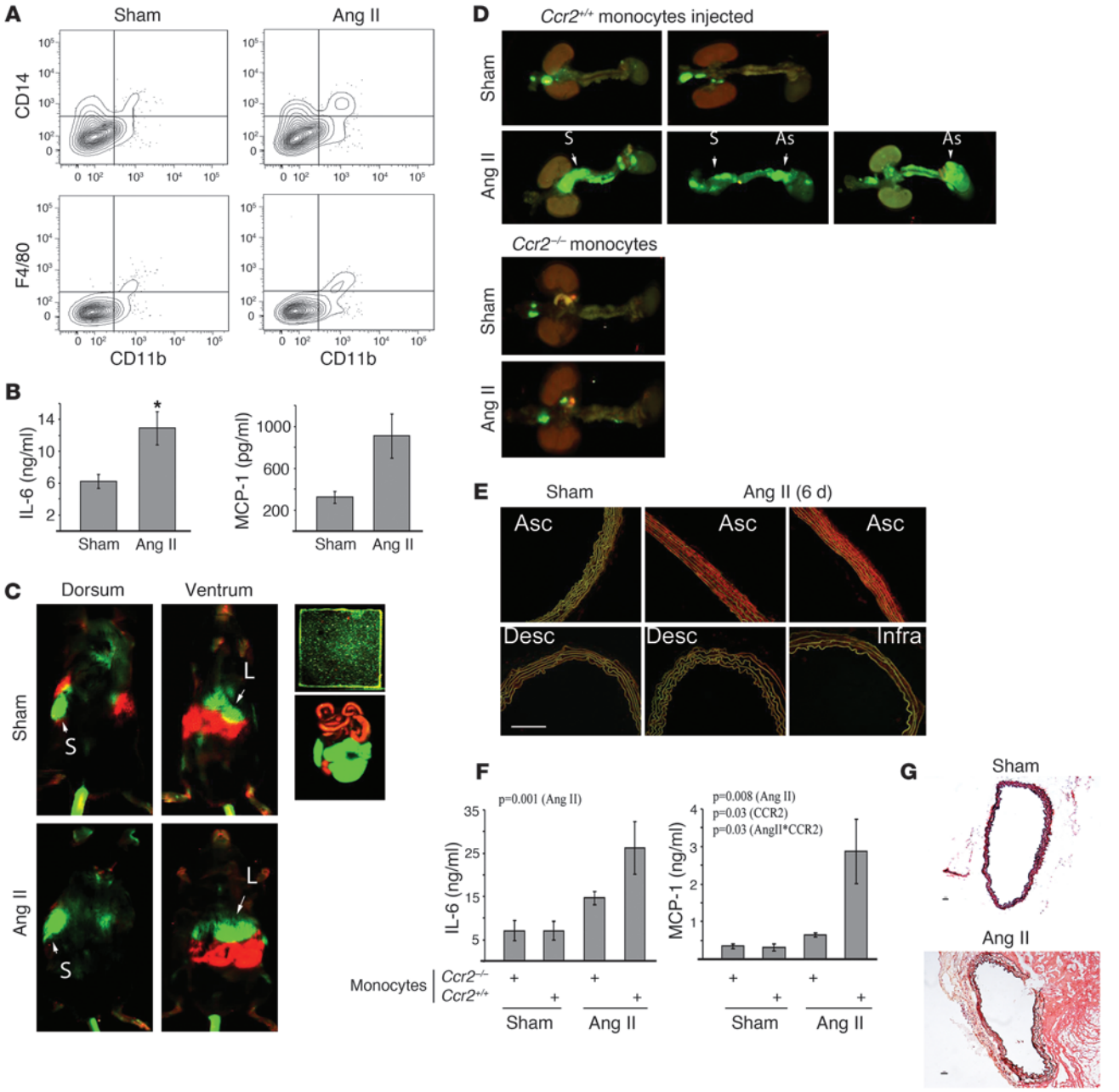

Figure 3

Ccr2$^{-/-}$ mice develop blunted responses to Ang II, but adoptive transfer of *Ccr2*$^{+/+}$ monocytes restores cytokine secretion and dissection. (**A**) Quantitation of aortic CD14^{+}CD11b^{+}F4/80^{+} macrophages in sham- and Ang II–treated *Ccr2*$^{-/-}$ mice. (**B**) Secreted IL-6 and MCP-1 concentrations in aortic explants culture from sham- (n = 6) or Ang II–infused (n = 7) *Ccr2*$^{-/-}$ mice. Data are mean ± SEM. *P < 0.03 versus sham treatment (Student's t test). (**C**) Whole-animal imaging of DiR800-labeled *Ccr2*$^{+/+}$ monocytes in *Ccr2*$^{-/-}$ mice with or without Ang II treatment. Monocytes (green) homed to the spleen (S), dorsal; liver (L), ventral. Nonspecific intestinal autofluorescence is shown in red. Monocyte labeling efficiency in vitro is shown (top right). (**D**) Aortic preparations from *Ccr2*$^{-/-}$ mice receiving *Ccr2*$^{-/-}$ or *Ccr2*$^{+/+}$ monocytes were imaged. The suprarenal (S) and the aortic root/ascending aorta (As) regions are shown for 3 separate animals (see Supplemental Figure 7). (**E**) In situ DHE staining. Aortas from control or Ang II–infused mice (6 days) were separated into ascending, descending and supra- and infrarenal segments and incubated in DHE (oxidation is shown in red). Nuclei are DAPI stained (blue). Scale bar: 50 μm; original magnification, ×200. (**F**) Secreted IL-6 and MCP-1 concentrations were measured in aortic explant medium from sham- (n = 5) or Ang II–infused (n = 6) *Ccr2*$^{-/-}$ mice receiving *Ccr2*$^{+/+}$ or *Ccr2*$^{-/-}$ monocytes. Data are mean ± SEM. Significant values are shown (2-way ANOVA, with P values representing Ang II effect, Ccr2 genotype effect, and interaction effect of Ang II with genotype [AngII*CCR2]). (**G**) Aortic cross sections after Ang II infusion in *Ccr2*$^{-/-}$ mice. Top: sham-treated; bottom: *Ccr2*$^{+/+}$ monocyte–infused. Scale bars: 10 μm; original magnification, ×100.

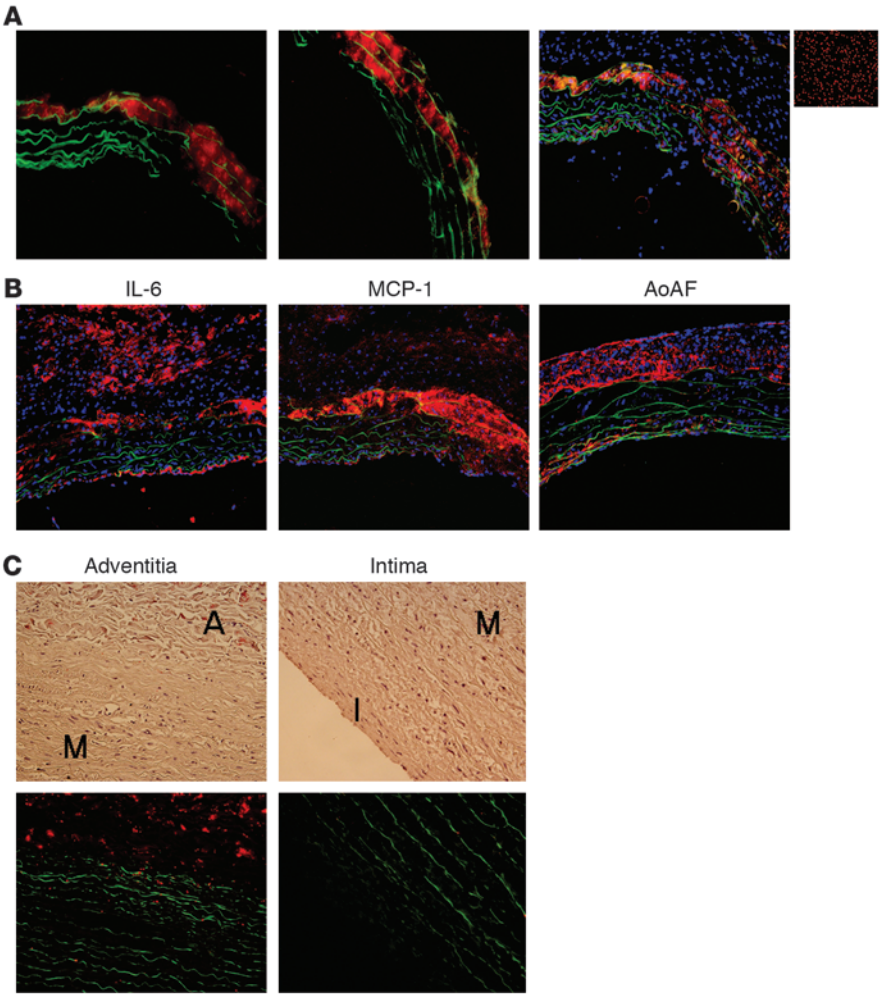

Figure 4
Localization of macrophages, AoAFs, and cytokines in mouse ascending aorta and IL-6 in sporadic type A aortic dissection in human tissue. (**A**) PKH26-labeled *Ccr2*$^{+/+}$ monocytes (red) were transferred into *Ccr2*$^{-/-}$ mice. Labeled macrophages are detected in cross sections of an ascending dissecting aneurysm invading the media from the adventitia/media border along with disruption of elastic lamellae at the dissection. Nuclei are DAPI stained (blue; right). The small image shows monocytes labeled in vitro. (**B**) Immunofluorescence staining for IL-6, MCP-1, and AoAF in transverse cryosections (6 μm) of ascending aorta from Ang II–treated *Ccr2*$^{-/-}$ mice injected with *Ccr2*$^{+/+}$ monocytes (positive staining is shown in red). Nuclei are DAPI stained (blue). Elastic lamellae are green. (**C**) Human type A sporadic dissection was stained for IL-6 (red). Note IL-6 staining is predominantly adventitial (left) and not in the medial or intimal (right) layers. Elastic lamellae are green. Hematoxylin was used as the counterstain. A, adventitia; M, media; I, intima. Original magnification, ×200.

aortic explant secretion of TNF-α (data not shown). Remarkably, the transfer of *Ccr2*$^{+/+}$ monocytes caused aortic dissections in 4 of 7 (57.1%) *Ccr2*$^{-/-}$ mice infused with Ang II (Figure 3G), which was significant compared with sham-treated mice ($P < 0.05$, Fisher's exact test, 1-sided).

Next, we examined aortic tissue from these mice using fluorescence microscopy (to detect the PKH26 dye). Aortic cross sections at the root/ascending aorta region showed monocyte-derived macrophages invading the media from the media-adventitia border and colocalizing with tears in the medial elastic lamellae, structures detected by green autofluorescence (Figure 4A). These macrophages were identified based on the red fluorescence of the PKH26 dye without any additional staining. DAPI nuclear staining confirmed that the red PKH26 fluorescent signal represented cells. No red fluorescence was detectable in aortic cross sections from non–monocyte-injected mice (data not shown). Also in the ascending aorta, IL-6 was detected mostly in the adventitia, with some staining in the intima, while MCP-1 was predominantly in the outer media and the media-adventitia border, with some low, diffuse staining in the adventitia (Figure 4B). Thickening of the adventitia was observed along with increased staining for adventitial fibroblasts.

Sporadic human thoracic aortic aneurysm and dissection also express IL-6 in the adventitia. Although circulating IL-6 is increased with thoracic and abdominal aneurysms in humans, the location of IL-6 production in the aorta is unclear. Thus, we sought to detect IL-6 in human thoracic aneurysm and dissection. In aortic cross sections, IL-6 was detected by immunofluorescence microscopy predominantly in the adventitia (Figure 4C), with little to no IL-6 staining observed in the media and intima. In addition, little to no detectable staining was observed in non-dissected aortic samples (data not shown). These results confirm our findings from previous studies in rodents indicating that the adventitia represents the source of the most abundant local IL-6 cytokine production in vascular inflammation (29).

Il6$^{-/-}$ *mice have reduced inflammatory responses to Ang II.* IL-6 is one of the most highly induced cytokines in aneurysms from human and experimental animals (17–19, 29), but its contribution to aortic disease has not been clearly defined. To study its role in our short-term Ang II infusion model, we infused *Il6*$^{-/-}$ mice with Ang II for 6 days. We did not observe aortic dissections in this time frame. Concomitantly, levels of secreted aortic MCP-1 increased only 3.4-fold (Figure 5A), which is significantly reduced compared with the much larger Ang II–induced increases in WT animals (Supplemental Figure 1; $P < 0.03$, 1-way ANOVA with Tukey's post-hoc test).

To determine whether the reduced responses were associated with macrophage number and phenotypes, sham- and Ang II–treated *Il6*$^{-/-}$ aortas were digested to characterize their macrophages. The number of macrophages increased by only 3.7-fold with treat-

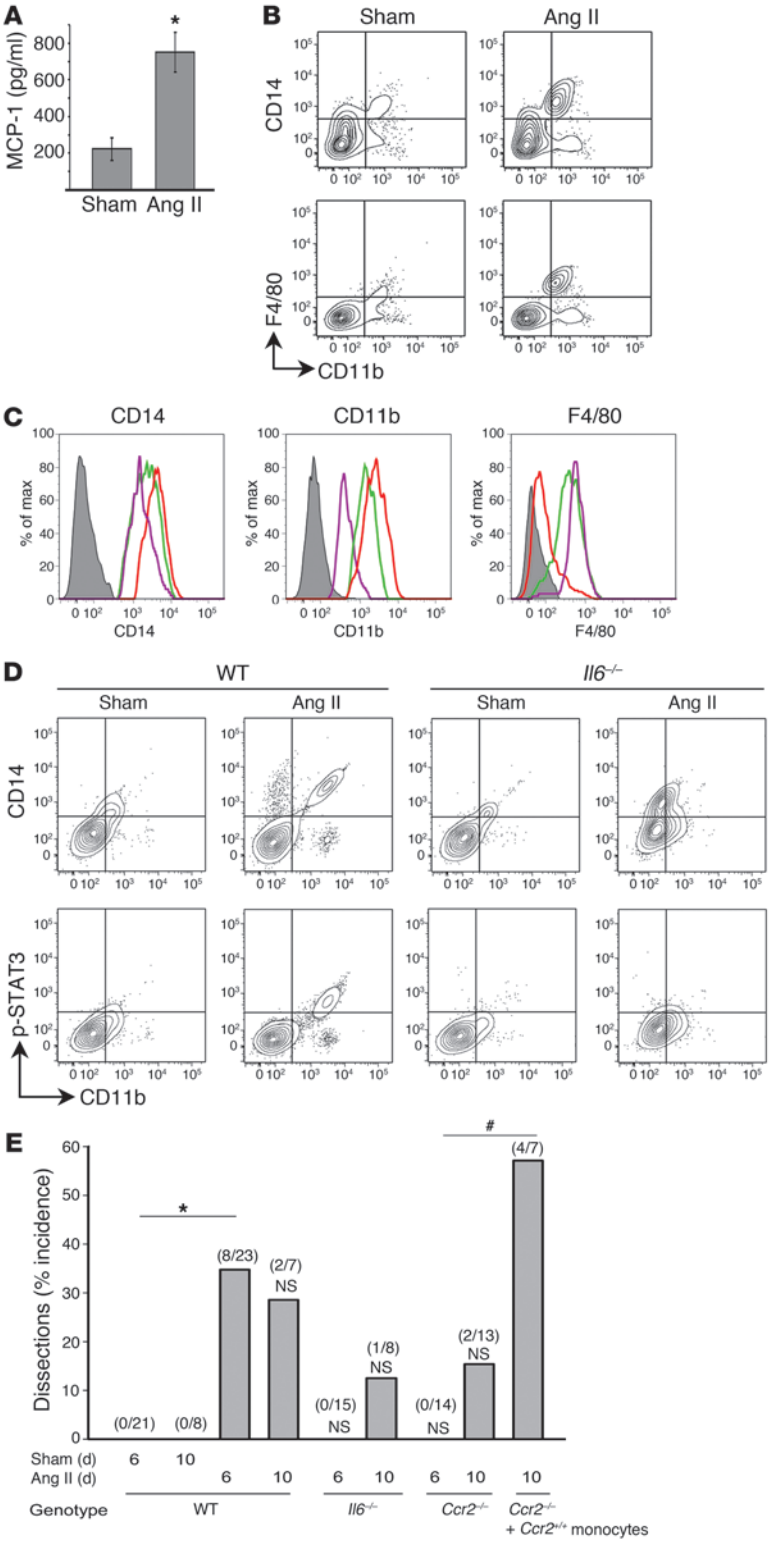

Figure 5

Il6$^{-/-}$ mice develop blunted responses to Ang II. (**A**) Secreted MCP-1 was measured in aortic explant medium from sham- or Ang II–infused *Il6*$^{-/-}$ mice after 6 days (n = 7 per group). Data are mean ± SEM. *P < 0.05 compared with sham-treated (Student's t test). (**B**) Resident CD14^{+}CD11b^{+}F4/80^{+} macrophages are present in aortas of *Il6*$^{-/-}$ mice. Increased numbers were recruited to the aorta of Ang II–infused mice. No aneurysms were seen. (**C**) Histograms comparing CD14, CD11b, and F4/80 expression on aortic macrophage populations in Ang II–infused WT mice (green curve), WT mice with dissecting aneurysm (red curve), and Ang II–infused *Il6*$^{-/-}$ mice (purple curve). (**D**) Aortic macrophages were stained with anti–p–Tyr705-STAT3 Ab (p-STAT3). CD14^{+}CD11b^{+} macrophages in sham-treated WT mice were p-STAT3^{-}, while those in Ang II–infused WT mice were p-STAT3^{+}. CD14^{+}CD11b^{+} macrophages in both sham- and Ang II–infused *Il6*$^{-/-}$ mice were p-STAT3^{-}. (**E**) Summary of dissection incidence by genotype. For each genotype, the incidence of aortic dissection is shown for 6- and 10-day Ang II infusion. In parentheses, the number of dissections are indicated as the numerator; the denominator is total number analyzed. Sham-infused mice for each genotype at each time point exhibited no dissections (not shown). *P < 0.004 versus sham infusion for 6 days, Fischer's exact test, 1-sided; $^{\#}P$ < 0.01 versus *Ccr2*$^{-/-}$, Fischer's exact test, 1-sided; NS, not significant compared with sham-treated for same genotype and day.

ment, and the percentage of macrophages in the treated aortas was half that observed in aortas from Ang II–infused WT mice (Table 1). Although macrophages from sham-infused aortas in the *Il6*$^{-/-}$ background had CD11b and CD14 staining similar to that in sham-infused WT aortas, the macrophages from the Ang II–treated *Il6*$^{-/-}$ aortas were distinctly different (Figure 5B). Here we noted that the CD11b staining did not reach the same levels in response to Ang II as in macrophages from WT mice with treatment or dissection, despite normal expression of F4/80 (Figure 5C). Staining for CD14 was on the lower end of the range observed in WT mice.

These data suggest that macrophages were signaling in response to IL-6 to alter their expression of cell-surface markers. To test this, we examined the status of IL-6 signaling pathway activation. IL-6 activates gp130 signaling and Jak/Tyk tyrosine kinases to induce STAT3 phosphorylation at Tyr705. CD14^{+}CD11b^{+} macrophages were positive for p–Tyr705-STAT3 in treated WT mice, but not in sham-infused mice (Figure 5D). Neither sham- nor Ang II–infused mice in the *Il6*$^{-/-}$ background had detectable p–Tyr705-STAT3^{+} macrophages. A population of CD11b^{+} cells was also detected, but they were not positive for p–Tyr705-STAT3. These data suggest that local IL-6 is directly signaling to aortic CD14^{+}CD11b^{+} macrophages, and this signaling pathway is required for formation of aortic dissections.

A summary of the effect of Ang II in the different genotypes is shown in Figure 5E. In WT mice, Ang II induced a statistically significant increase in aortic dissections after 6 days of infusion (P < 0.004, Fischer's exact test). By contrast, deficiency of either IL-6 or CCR2 reduced this early incidence of Ang II–induced aortic dissections compared with those seen in WT mice. This reduction in dissections was significant at 6 days for both *Il6*$^{-/-}$ and *Ccr2*$^{-/-}$ genotypes (P < 0.05, Fischer's exact test). Importantly, the reduction in dissections seen in *Ccr2*$^{-/-}$ mice was lost upon infusion of *Ccr2*$^{+/+}$ monocytes. We therefore conclude that both IL-6 and MCP play an important role early in the development of aortic dissections.

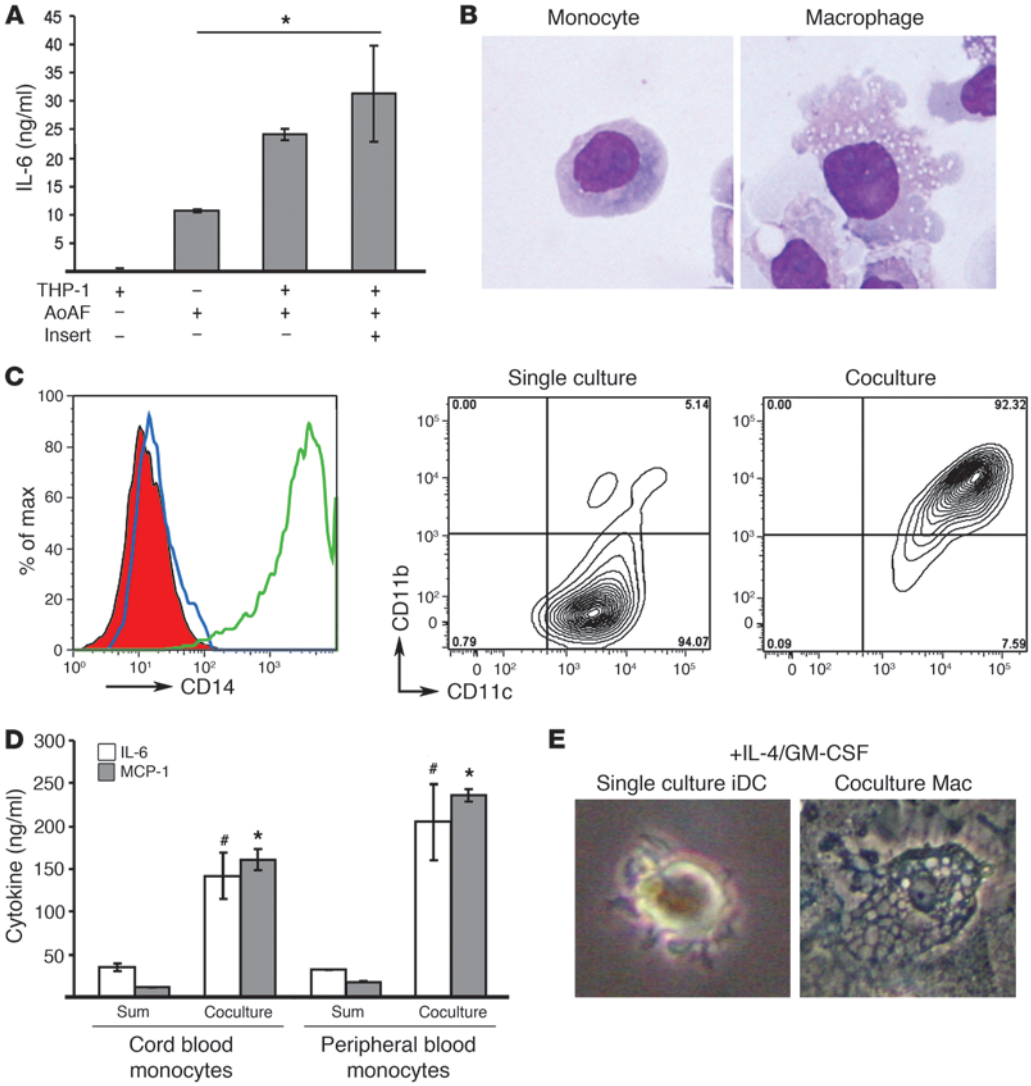

Figure 6

Coculture of monocytes with AoAFs induces IL-6, MCP-1, and monocyte-to-macrophage differentiation. (**A**) THP-1 monocytic cells cultured with human AoAFs induce IL-6 independent of cell-cell contact. Data are mean ± SD (n = 3 per group), compared by 1-way ANOVA (P = 0.003) with Tukey's post-hoc test for significance between the groups. *P < 0.05 versus AoAF alone. (**B**) Giemsa staining shows morphology of THP-1 monocytic cells and derived macrophages from coculture. Original magnification, ×200. (**C**) Histogram of CD14 staining on THP-1 cells (blue curve) and derived macrophages in the presence of IL-4/GM-CSF (green curve). Isotype control curve is solid red. CD11b staining is also increased in THP-1–derived macrophages (right) compared with THP-1 cells (middle). (**D**) Coculture of umbilical cord blood monocytes and adult peripheral blood monocytes induces IL-6 and MCP-1 compared with the sum of cytokines produced in individual cultures in the presence of IL-4/GM-CSF. Data are mean ± SD. #P < 0.05 versus sum of IL-6 levels from single cultures; *P < 0.05 versus sum of MCP-1 levels from single cultures, Student's t test. (**E**) Culture of peripheral blood monocytes in IL-4/GM-CSF produces iDCs, but in coculture with human AoAF, cells differentiate into macrophages. Original magnification, ×200.

Monocyte–adventitial fibroblast interaction potentiates cytokine expression and macrophage differentiation. Since macrophages are mostly recruited to the adventitia, and adventitial fibroblasts increase with disease formation in vivo, we hypothesized that the infiltrating monocytes/macrophages interact with adventitial fibroblasts to potentiate IL-6 production. To test this hypothesis in vitro, we cultured monocytes with primary human AoAFs. Although THP-1 cells do not produce IL-6 (<3.2 pg/ml), in the presence of AoAF, the levels of IL-6 were increased 2.3-fold. To determine whether there was a requirement for direct interaction, we cocultured THP-1 monocytes with AoAF separated by a Transwell insert. The level of IL-6 in the Transwell-separated coculture medium was still significantly higher (3-fold) than that from AoAFs cultured alone (P < 0.05; Figure 6A). Overall, our data indicate that THP-1–AoAF interaction increases IL-6 secretion but this phenomenon is not mediated by direct cell-cell interaction.

Moreover, we found that the fibroblast interaction differentiated THP-1 monocytic cells into macrophages, characterized morphologically by adherence to the fibroblasts and numerous cytoplasmic vacuoles (Figure 6B). We then characterized this differentiation based on expression of CD14 and CD11b. Since CD14 is also highly expressed on monocytes, THP-1 cells were treated with IL-4

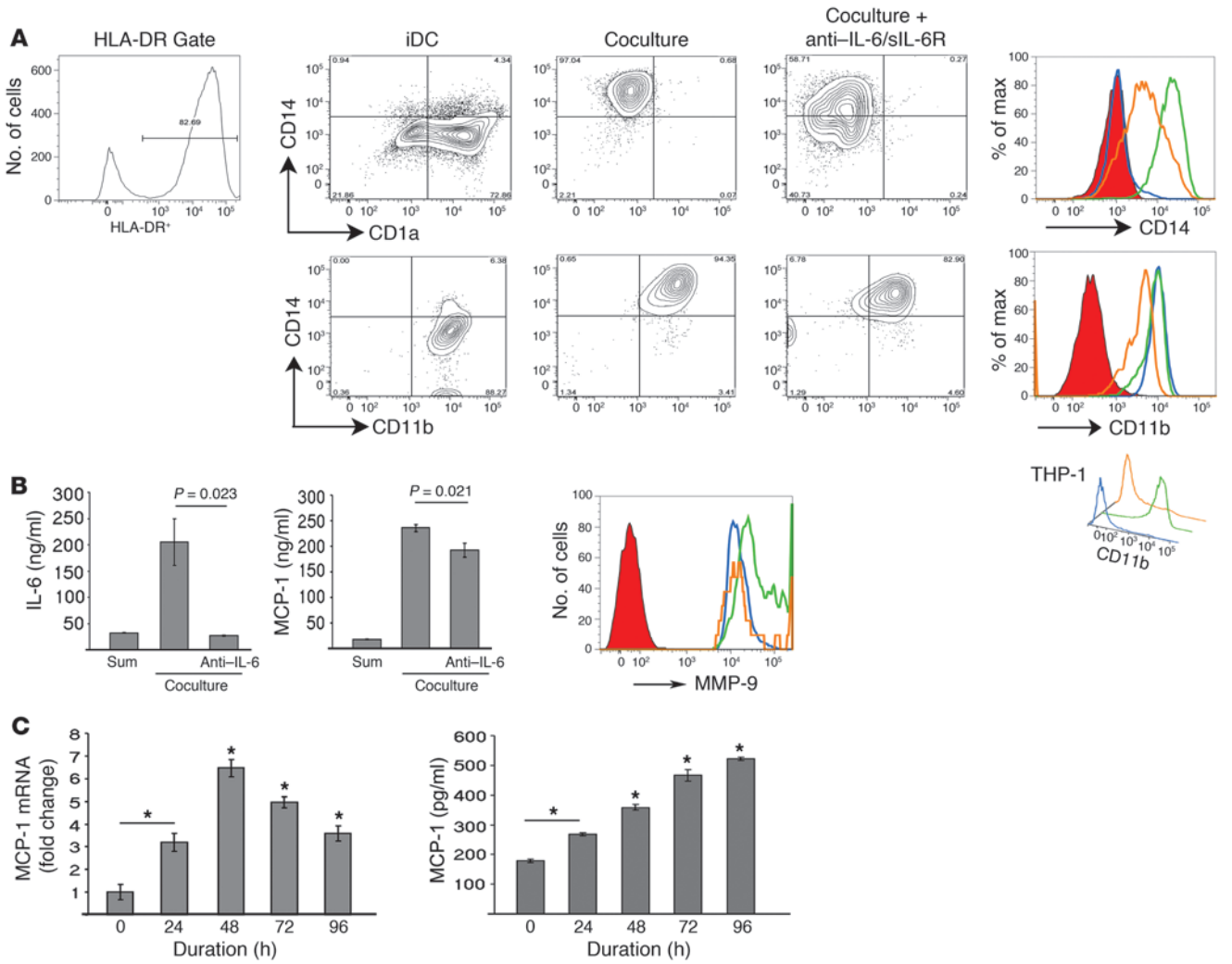

Figure 7

Monocyte-to-macrophage differentiation in coculture is IL-6 dependent. (**A**) Top: IL-4/GM-CSF induces peripheral blood monocytes to become CD1a$^+$CD14$^-$ (iDCs). Coculture with human AoAFs differentiates the monocytes into CD1a$^-$CD14$^+$ macrophages (macrophages were separated from fibroblasts by HLD-DR$^+$ gating). Addition of anti–IL-6 and anti–sIL-6R Abs reduces CD14 expression. Histogram compares CD14 staining on iDCs (blue), macrophages (green), and cells in the presence of anti–IL-6/sIL-6R (orange). Isotype control is red. Bottom: Parallel experiments show that the iDCs are CD14$^-$CD11b$^+$, macrophages are CD14$^+$CD11b$^+$, and inhibition of IL-6 reduces CD11b expression on macrophages. Inset (bottom right): IL-6 inhibition reduces CD11b expression in THP-1 cells. (**B**) Inhibition of IL-6 in coculture (left) reduces levels of MCP-1 and MMP-9 (histogram with same color coding as in **A**). (**C**) IL-6 stimulates THP-1 monocytic cells to increase MCP-1 mRNA up to 48 hours, while secreted MCP-1 continues to increase up to 96 hours. *$P \leq 0.001$ versus baseline ($n = 3$). Data in **B** and **C** are mean ± SD and compared using 1-way ANOVA with multiple comparisons and Tukey's post-hoc test for significance between groups.

and GM-CSF to downregulate constitutive CD14 expression (44, 45). In this cytokine environment, monocytes will differentiate into CD14$^-$ immature dendritic cells (iDCs) by default. IL-4/GM-CSF–treated monocytes were CD14$^-$ and CD11c$^+$CD11b$^-$, but in the presence of AoAFs, there were CD14$^+$ and CD11c$^+$CD11b$^+$ macrophages (Figure 6C). These findings were confirmed with primary human monocytes. IL-6 was increased by 3.5- and 6.3-fold when umbilical cord blood or adult peripheral blood monocytes were cocultured with AoAFs, respectively, as compared with the sum of IL-6 produced from each cell type alone (Figure 6D). Surprisingly, we observed that MCP-1 was induced by 14.0- and 13.2-fold, respectively. Figure 6E shows the morphological differentiation of primary monocytes into iDCs in single culture with IL-4/GM-CSF but into macrophages in the presence of AoAFs and the same cytokine environment. These data indicate that AoAFs secrete paracrine factor(s) that induce IL-6 and MCP-1 production, promoting monocyte-to-macrophage differentiation.

To determine whether the differentiation to macrophages was IL-6 dependent, we added anti–IL-6 and anti–soluble IL-6 receptor (anti–sIL-6R) Abs to the coculture experiments. In these experiments, gating for HLA-DR was performed to separate the monocytes/iDCs/macrophages from fibroblasts. Peripheral blood monocytes became CD1a$^+$CD14$^-$ iDCs in single culture but CD1a$^-$CD14$^+$ macrophages in coculture. Neutralizing IL-6 Ab decreased CD14 expression on macrophages in coculture (Figure 7A). In a parallel experiment, peripheral blood monocytes were found

to be $CD14^-CD11b^+$ iDCs in single culture but $CD14^+CD11b^+$ macrophages in coculture. CD11b expression on macrophages was decreased with neutralization of IL-6. The downregulation of CD11b was seen more clearly in THP-1 cells (Figure 7A, inset). The discrepancy between expression of CD11b on peripheral blood–derived iDCs and THP-1 cells cultured with IL-4/GM-CSF might be due to the presence of IL-6 in the culture medium of primary iDCs. Although neutralization of IL-6 was only partial in these experiments, it was found to decrease amounts of secreted MCP-1 in coculture and inhibit MMP-9 induction (Figure 7B). To directly demonstrate that IL-6 can upregulate MCP-1 expression, we stimulated THP-1 monocytic cells with 8 ng/ml recombinant IL-6 for 96 hours. While MCP-1 mRNA increased to a maximum at 48 hours and then decreased but was still elevated at 96 hours, the amount of secreted MCP-1 protein gradually increased up to 96 hours (Figure 7C). These data indicate that IL-6 potentiates macrophage differentiation and activation upstream of MCP-1.

Discussion

In this study, we developed an animal model of Ang II–induced vascular inflammation that resulted in acute thoracic and suprarenal aortic aneurysms and dissections in the absence of the confounding effects of hyperlipidemia. In this model, we confirm that Ang II induces local production of IL-6 and MCP-1 secretion, ROS formation, monocyte recruitment, and macrophage activation characterized by $CD14^{hi}CD11b^{hi}F4/80^-$ cell-surface staining. Using adoptive transfer studies, we identified 2 regional sites within the aorta for monocyte uptake and adventitial accumulation that were dependent on Ang II stimulation and CCR2 signaling. This process of monocyte recruitment potentiates adventitial IL-6 secretion seen the animal model and in sporadic thoracic aortic dissections in humans. Our work further suggests that this process is governed by paracrine factors released during monocyte–aortic fibroblast interactions in vitro. Specifically, our work suggests that IL-6 regulates monocyte-to-macrophage differentiation and activation in the aorta along with MCP-1 production and MMP expression. Collectively, our data demonstrate that IL-6 coordinates vascular inflammation via MCP-1 upregulation and macrophage recruitment and activation; these findings may be relevant to IL-6's role in other inflammatory cardiovascular diseases in addition to aortic aneurysms and dissections.

Ang II infusion is a potent inducer of vascular inflammation, and its physiological effect has been extensively studied in mouse models. Those studies have largely employed hyperlipidemic *Apoe*$^{-/-}$ and *Ldlr*$^{-/-}$ mice, in which the blood pressure–independent effects of Ang II include both acceleration of the formation of atherosclerosis and induction of suprarenal aneurysms (29, 37, 38, 46). In these models, the presence of hyperlipidemia induces ROS, apparently to sensitize the vessel to the inflammatory actions of Ang II and is well known to increase the incidence of abdominal aneurysms (39, 47). These genetic backgrounds make the isolated study of the pathogenic mechanisms of Ang II on aortic aneurysm and dissection difficult. In this study, we found that Ang II infusion into older C57BL/6J mice reproducibly produced both suprarenal and ascending thoracic aneurysms and dissections. The thoracic dissections that we observe are similar to human type A dissections based on their location in the ascending aorta and the formation of false lumens resulting in intravascular hematomas. However, these models differ in that the dissections enter the adventitia, whereas human type A dissections create false lumens within the media.

Our study extends previous work showing that Ang II infusion into young C57BL/6 mice induces macrophage recruitment, but no apparent dissections (12), and that Ang II induces suprarenal abdominal aortic aneurysms in older mice (39). Comparison of the vascular cytokine response between the 2 age groups showed that older mice had enhanced cytokine reactivity to Ang II infusion (Figure 1C). Why older mice are more sensitive to Ang II remains unknown, although we speculate that mitochondrial dysfunction associated with aging may contribute to enhanced ROS formation, thereby enhancing chemokine production, with subsequent monocyte recruitment and aortic remodeling. We note that aging is a major risk factor for human abdominal aortic aneurysms (48).

It is well established that Ang II infusion enhances macrophage recruitment and accelerates atherosclerosis (47, 49, 50), in which the roles of monocyte-derived chemokines osteopontin and MCP-1 have been implicated. However, this work has been limited by the inability to systematically quantitate macrophage number due to their reliance on histochemical methods sensitive to regional differences in monocyte uptake. Here, we adapted an established method of tissue dissociation and quantitative flow cytometry to circumvent these limitations (51). In our characterization of this isolation method, the reduction in residual aortic tissue as a function of digestion time indicates that the method is effective in dissolution of the aortic structural components, and the loss of cellular β-actin staining suggests that the method efficiently extracts cellular constituents (Supplemental Figures 1 and 2). Nevertheless, in the analysis of SSC-A, a number of events stained positive for ethidium homodimer, indicating that a substantial fraction of the total cells were nonviable. This finding is consistent with the work of others (51), and the studies together suggest that we are underestimating the total aortic cell number. However, we note that measurement of cellular viability in the monocyte gating window clearly show that the monocyte population is largely composed of viable cells, the primary end point of this study (Figure 2A and Supplemental Figure 4). An important caveat of our study is that we lack the ability to address experimentally whether the aortic dissolution technique preferentially enriches certain cell populations. This question will require further work and development of quantitative morphometric analysis of tissues. However, we note that the finding of enhanced macrophage recruitment indicated by the flow cytometric assays is independently supported by the enhanced recruitment of vital dye-labeled *Ccr2*$^{+/+}$ macrophages (Figure 3D), the latter representing a method that does not rely on cellular dissolution.

Given these caveats, our study shows that Ang II is a potent inducer of macrophage populations in the remodeling aorta, which dramatically increased up to 32% of the total recoverable cell population in animals with acute dissections. Moreover, our ability to measure activation state showed that resident aortic macrophages were $CD14^+CD11b^+F4/80^+$ in sham-treated WT mice, while *Ccr2*$^+$ monocytes recruited into the aorta by Ang II became macrophages that expressed higher CD14 and CD11b but were surprisingly $F4/80^-$, a signature indicating cellular activation, in dissecting aortas. In contrast, *Il6*$^{-/-}$ mice treated with Ang II for 6 days did not develop aneurysms and had $CD14^{lo}CD11b^{lo}F4/80^+$ aortic macrophages. Together with the finding that macrophages stain for p–Tyr705-STAT3 in an IL-6–dependent manner, this suggests to us that local IL-6 may be responsible for differentiating monocytes to become $CD14^{hi}CD11b^{hi}$ $F4/80^-$ activated aortic macrophages that further induce IL-6, express MCP-1, and cause

aortic dissections. Selective targeting of these pathogenic macrophages may have therapeutic and diagnostic relevance.

We and others have reported that macrophage uptake occurs predominantly in the tunica adventitia in both humans and animal models (27, 29, 37, 40, 50, 52–56), in association with elastic lamellar tears. Initial adventitial recruitment is mediated by the potent chemotactic properties of MCP-1, followed by subsequent medial invasion (3, 4, 40, 57, 58). This process may be facilitated by adventitial IL-6 secretion to upregulate CD11b expression. CD11b is an integrin mediating monocyte/macrophage adhesion, migration, and phagocytosis (59–61) that complexes with CD18 to become an $\alpha_M\beta_2$ integrin receptor known as Mac-1. Importantly, Mac-1 ligands, fibrinogen, factor X, and ICAM-1 are upregulated by IL-6 *trans* signaling in vivo (62, 63). CD11b can form a complex with urokinase-type plasminogen activator receptor (uPAR) expressed on activated macrophages (64–70). The expression of the uPAR ligand urokinase-type plasminogen activator (uPA) increases 13-fold in aneurysmal tissue of Ang II–infused *Apoe*$^{-/-}$ mice, where it cleaves plasminogen to produce MMP-activating plasmin (39, 40, 71). We speculate that Ang II's effect of inducing IL-6 may increase ICAM-1 and augment CD11b expression on macrophages to bind uPAR. Subsequent association with uPA may facilitate dissociation, allowing for migration, and MMP activation. In fact, blockade of CD11b has been shown to reduce vessel wall macrophage infiltration (72). The activity of IL-6, therefore, creates an environment where macrophages can attach, migrate, and degrade tissue from the adventitia inward.

Vital staining experiments in our rodent model revealed that monocytes preferentially home to ascending and suprarenal sections of the aorta, representing the 2 major sites for dissection. This finding underscores our previous suggestion that monocyte recruitment is not uniform but rather occurs in specific locations. In this regard, we have noticed extensive increases in volume of the vasa vasorum in these areas (data not shown), explaining the propensity for preferential monocyte recruitment. It remains unknown why these specific regions are prone to neovascularization or the mechanisms controlling this process. These 2 regions of increased IL-6 are also sites for ROS generation, suggesting linkage between monocyte recruitment and ROS production (39, 40). Our finding that the Ang II–induced medial elastic lamellar disruption and dissection in the abdominal aorta also occur in the presence of macrophages suggests that macrophages may be involved late in the process of aortic dilation and that regional uptake of monocytes, rather than inherent regional vessel properties, may be of primary influence in selecting the site for aortic dilation (37, 50, 73). Another group has shown that Ang II enhances thoracic aorta dissections in *Apoe*$^{-/-}$ mice (74); our study is the first to our knowledge to demonstrate this phenomenon in WT mice. This is an important observation, because human aneurysms are commonly found in this thoracic area. These data clearly demonstrate the important role of regional recruitment of CCR2^{+} monocytes in vascular inflammation and dissecting aneurysm disease.

Mechanistically, Ang II infusion induces local production of MCP-1 and IL-6 via defined signal transduction pathways (36). Although production of these 2 cytokines has been thought to be relatively independent, our data suggest that IL-6 and MCP-1 secretion are actually codependent. Specifically, Ang II infusion into mice of the *Ccr2*$^{-/-}$ background reduced IL-6 and MCP-1 secretion, which was restored to WT levels by infusion of physiologically relevant numbers of CCR2^{+} monocytes (75). Moreover, this adoptive transfer also restored aortic dissection rates to levels indistinguishable from those of WT mice. Similarly, we found that Ang II–induced MCP-1 expression was reduced in *Il6*$^{-/-}$ mice. Our experiments investigating interactions between primary AoAFs and monocytes reproduced these in vivo observations. Here, IL-6 and MCP-1 secretion were potentiated by cellular interactions in coculture. AoAF interactions further induced CD14 and CD11b and monocyte-to-macrophage differentiation in an IL-6–dependent manner. Taken together with the in vivo observations that IL-6, MCP-1, macrophages, and fibroblasts are predominantly localized to the tunica adventitia, these findings support the conclusion that adventitial fibroblast-monocyte interactions potentiate Ang II–induced cytokine release and aortic dissection. These data suggest the cellular basis for an inducible IL-6/MCP-1 amplification loop important in vascular inflammation.

Although our data clearly indicate that IL-6 or CCR2 deficiency reduces the early onset of aortic dissections, we note that these genotypes do not totally protect mice from aortic dissection with longer (10-day) infusions (Figure 5E). When we infused CCR2 and IL-6–knockout mice for 10 days, we found that 2 of 13 (15.4%) *Ccr2*$^{-/-}$ mice and 1 of 8 (12.5%) *Il6*$^{-/-}$ mice developed aortic dissection, which is still half the incidence observed in WT mice after 6 days of infusion. Although this trend suggests a reduced rate of aortic dissection, because our study was designed to focus on early Ang II–induced events, it was not sufficiently powerful to examine the effect of chronic Ang II infusions. More work will be required to establish the significance of chronic Ang II infusion in these genetic backgrounds. Nevertheless, our observations suggest that early development of Ang II–induced aneurysm and aortic dissection formation is partly CCR2 and IL-6 independent. These findings underscore our understanding that this is a complex phenotype, dependent on a multitude of processes whose interaction ultimately results in a loss of aortic wall integrity. Nevertheless, these results more importantly suggest that MCP-1 and IL-6 signaling accelerates the development and increases the incidence of aneurysm and aortic dissections.

In summary, we suggest that interaction between AoAF and macrophages provides a IL-6/MCP-1 amplification loop for acceleration of vascular inflammation. We propose that IL-6 is induced when monocytes are recruited to the adventitia, coming into close proximity to adventitial fibroblasts. Increased IL-6 then promotes monocyte differentiation into mobile, activated macrophages that secrete MCP-1 and MMPs, which facilitate invasion from the adventitia into the media and recruit more monocytes into the adventitia, amplifying the process. These observations suggest potential sites for therapeutic intervention to effectively disrupt vascular inflammation common to many cardiovascular diseases.

Methods

Animal care and use. All animal experiments were approved by the Institutional Animal Care and Use Committee of the University of Texas Medical Branch Animal Resource Center. Male C57BL/6J WT and *Il6*$^{-/-}$ mice were obtained from The Jackson Laboratory. *Ccr2*$^{-/-}$ breeding pairs were from The Jackson Laboratory and bred in house. Age-matched male *Ccr2*$^{-/-}$ mice were used in all experiments. Both *Ccr2*$^{-/-}$ and *Il6*$^{-/-}$ mice were in the C57BL/6J background. For Ang II infusion, anesthetized mice received subcutaneous Alzet osmotic minipumps (Durcet Corp.) delivering either saline (sham) or Ang II (synthesized by the University of Texas Medical Branch peptide synthesis core) at 2,500 ng/kg/min for 6 or 10 days. Intravascular blood pressure was measured in ketamine-anesthetized mice

using carotid artery cannulation and external monitoring with a BP-100 intravascular blood pressure transducer (iWorx/CB Sciences).

Aortic explant and cytokine analysis. Ketamine-anesthetized mice were perfused with PBS via the left ventricle to remove blood from tissue, then hearts and aortas were excised in one piece and placed in sterile PBS, and periadventitial fat was removed. The entire aorta (approximately 4.4–5 cm) was dissected and immediately placed in 0.5 ml DMEM medium (Cellgro) containing 1× ITS (Sigma-Aldrich) and 0.1% BSA (Sigma-Aldrich) and incubated in a tissue culture hood at 37°C for 4 hours. In experiments where cytokine secretion was normalized to dry weight, aortas were removed from conditioned medium, with excessive liquid absorbed by sterile surgical gauze, and placed in a 55°C drying oven for approximately 72 hours until weights stabilized for measurement. Culture medium was frozen at –80°C until being assayed for IL-6 and MCP-1 using a multiplex, bead-based ELISA kit (Lincoplex/Millipore mouse or human adipocyte/cytokine panel) according to the manufacturer's instructions.

IHC and immunofluorescence. Slides containing frozen mouse aortic cross sections (6-μm) were immediately fixed with 4% PFA for 30 minutes, blocked using 0.1% Triton-X, 5% normal serum of the species producing the highly cross-absorbed Alexa Fluor 568–conjugated secondary Ab (Invitrogen) for 15 minutes at 37°C and then incubated with primary Abs at the following concentrations: 1:100 anti-CD11b (M1/70; eBioscience), 1:100 anti-fibroblast (ER-TR7; Bachem), 1:50 anti–MCP-1 (ECE.2; Abcam), 1:200 anti–IL-6 (eBioscience), and 1:200 anti-macrophage (MOMA-2; Abcam). Incubations were performed for 2 hours at 37°C or overnight at 4°C. After washing, secondary Abs were added at a dilution of 1:200 for 45 minutes at 37°C. Slides were then DAPI stained (Vector Laboratories). For human aortic tissue samples, discarded aortic tissue and deidentified clinical data from patients undergoing surgical aortic repair were obtained with informed consent under a protocol approved by the University of Texas Health Science Center Institutional Review Board. PFA-fixed, paraffin-embedded sections were taken from the ascending aorta above the sinuses of Valsalva. The sections were microwaved and stained using VECTASTAIN ABC-AP kit (Vector Laboratories) using a 1:100 dilution of anti–IL-6 Ab (clone 6708; R&D systems). Vector Red (Vector Laboratories) was used as substrate. Secondary Ab–only controls were used to determine staining specificity.

In situ DHE oxidation. Aortas from sham- or Ang II–infused mice were dissected, OCT embedded, and frozen in a methybutane/ethanol/dry ice bath. Frozen sections (8-μm-thick) were mounted on glass slides, rinsed in PBS, and incubated in 10 μM DHE (37°C, 30 minutes; Invitrogen). Then slides were DAPI stained, mounted, and photographed using a Texas red filter (488-nm excitation, 610-nm emission).

Aortic digestion. Aortas were minced into 3- to 4-mm pieces and placed in 1-ml digestion solution containing 1.25 mg/ml collagenase (Sigma-Aldrich), 50 μg/ml porcine pancreatic elastase (Sigma-Aldrich), and 5 mM $CaCl_2$ in 0.9 ml base solution of Accumax (Innovative Cell Technologies). Aortic tissue was digested at room temperature with agitation for 1–4 hours. After digestion, cells were washed in FACS buffer (0.5% BSA, 0.02% NaN_3 in PBS) at 300 *g* for 5 minutes. Blocking and flow cytometry are described below. For samples with substantial rbc contamination, an rbc lysis step was performed after the initial wash. For detection of p-STAT3, aortas were digested in the presence of phosphatase inhibitors (5 mM depolymerized sodium orthovanadate and 50 mM NaF). After digestion, cells were quickly washed and then fixed in 0.5% PFA for 10 minutes. Cell permeabilization was performed with 100% cold methanol for 10 minutes on ice, and all washes and incubations were done in the presence of phosphatase inhibitors.

Flow cytometry. Murine Fc receptors were blocked using Abs against mouse CD16/32 antigens (eBioscience) for 10 minutes on ice, and cells were washed, then resuspended in 100 μl FACS buffer. Fluorochrome-conjugated Abs (FITC-CD11b [M1/70], PE-CD14 [Sa2-8], APC-F4/80 [BM8] all from eBioscience; Alexa Fluor 647–p-STAT3 Y705 [4/P-Stat3] from BD Biosciences) and CCR2 (M-50; from Santa Cruz Biotechnology Inc.) were added for 30–45 minutes at room temperature. Corresponding isotype control Abs were added to "isotype samples" at the same concentrations as the Abs of interest. After incubation, samples were washed 3 times in FACS buffer, centrifuged at 300 *g* for 5 minutes, then fixed in 0.5% PFA and analyzed by FASCanto. Compensation was performed using positive samples containing aortic macrophages stained for 1 color. For indirect staining using an unconjugated primary Ab, a 1:2,000 dilution of the conjugated secondary Ab was used. Human cells were blocked with human serum and staining was performed as above with the following Abs: FITC-CD1a (HI149), PE-CD14 (61D3), PE-CD11c (clone 3.9), PE-Cy7–CD11b (ICRF44), and allophycocyanin–HLA-DR (APC–HLA-DR; LN3) all from eBioscience; and MMP-9 from Sigma-Aldrich. Debris and dead cells, defined by low forward scatter, were excluded from analysis. Data were analyzed with FlowJo or Cyflogic.

Monocyte isolation. Blood from C57BL/6J WT or *Ccr2*$^{-/-}$ mice as indicated was collected into EDTA-coated vials and erythrocytes lysed used rbc lysis solution (Invitrogen) for 5 minutes at room temperature. Cells were centrifuged at 1,000 *g* for 3 minutes to remove rbc lysis solution, and the leukocyte pellet was resuspended and washed in cell isolation buffer (2% heat-inactivated FBS, 2 mM EDTA in PBS) followed by centrifugation at 400 *g* for 10 minutes. Leukocyte counting was done by trypan blue exclusion. Negative isolation of monocytes was performed using the SpinSep Murine Monocyte Isolation Custom Kit according to the manufacturer's instructions (Stem Cell Technologies). Briefly, an Ab cocktail was added to the leukocytes at a ratio of 10 μl per 5×10^7 nucleated cells per ml, the cells were incubated at 4°C for 15 minutes and washed, and 250 μl of SpinSep Dense Particles was added per 5×10^7 cells. This cell/particle suspension was incubated on ice for 20 minutes with occasional mixing; the mixture was diluted with 6 ml of isolation buffer and gently layered on top of 4 ml of SpinSep Density Medium at room temperature. Centrifugation was performed for 10 minutes at 1,200 *g* at room temperature. The enriched cells from the interface were carefully removed, washed, and resuspended in PBS. Eight mice allowed the isolation of 1.5×10^6 monocytes, representing 7% of all leukocytes. The purity was greater than 95% as assessed by CD14 staining.

Labeling of mouse monocytes. Mouse monocytes were DiR800- (Invitrogen) and PKH26-labeled (Sigma-Aldrich) simultaneously. Briefly, cells were resuspended in 1 ml solution A of PKH26, 4 μM solution of PKH26 dye in 1 ml was made in solution B, and a 1:500 dilution of 10 mg/ml DiR800 was added. Solution A was combined with solution B, and the cells were incubated for 3 minutes at room temperature. The final concentration of PKH26 was 2 μM and of DiR800 was 0.01 mg/ml. After incubation, cells were washed with PBS 3 times.

Adoptive transfer of mouse monocytes and in vivo imaging. Monocytes (1.5×10^6) in 150 μl of PBS were injected via the mouse tail vein using a 26-gauge needle (BD), and 4 days later, mice were anesthetized, shaved, and scanned using a LICOR Odyssey imaging system with a 2- to 4-mm offset. For detection of labeled cells in the aorta, aortas were excised and placed in 60-mm culture dishes and scanned as above. For detection of PKH26, the aortic root/ascending aorta was embedded and quickly frozen in OCT on dry ice, and detection of PKH26 in 6-μm cross sections was performed with fluorescence microscopy.

Coculture. Coculture experiments were performed at a monocyte/fibroblast ratio of 4:1. Monocytes (500×10^3) were added to a culture of 125×10^3 adventitial fibroblasts in 1.5 ml RPMI medium containing 5% FBS for 5 days. For cytokine analysis, the medium was removed and kept at –80°C. For flow cytometry, cells were dislodged with 2 mM EDTA. IL-4 and GM-CSF were added to the culture medium at a concentration of 10

ng/ml every 3 days starting day 0 of coculture. For neutralization of IL-6, 10 mg anti–IL-6 and anti–sIL-6R Abs were added daily from day 0. For Transwell experiments, monocytes were added to the top of polycarbonate inserts with 0.4-μm pores, and the fibroblasts were grown on the bottom well (Corning Lifesciences).

Real-time PCR. RNA was extracted from 1×10^6 THP-1 cells using TriReagent (Sigma-Aldrich) according to the manufacturer's instructions, and 0.5 μg RNA was reverse transcribed using Superscript III (Invitrogen) according to provided directions. Real-time PCR reactions were performed in triplicate using 1 μl of resulting cDNA per 20 μl reaction volume containing iQ SYBR Green Supermix (Bio-Rad). The housekeeping gene GAPDH was used as control. Primers for human MCP-1/CCL2 were 5′-CATTGTGGCCAAGGAGATCTG-3′ (forward) and 5′-CTTCGGAGTTTGGGTTTGCTT-3′ (reverse). PCR was performed on the MyiQ system (Bio-Rad) according to preset protocol. MCP-1 mRNA was analyzed by the ΔΔCt method.

Data analysis. Data are reported as mean ± SD or mean ± SEM as indicated. Differences between 2 groups were analyzed by Student's *t* test (2-tail, assuming unequal variances). Two-way ANOVA was performed separately for IL-6 and MCP-1, looking for an age as well as a treatment effect. One-way ANOVA was performed when looking for time differences due to IL-6 or MCP-1. This was followed by Tukey's post-hoc test to determine significance. Fisher's exact test was performed on the proportion data for ascending and suprarenal aortic dissections to determine significance at different time points because of small group size. In all cases, *P* values less than 0.05 were considered significant.

Acknowledgments

This work was supported by NIH grants P50 HL083794 (to D. Milewicz and A.R. Brasier), HL70925 (to A.R. Brasier), and DK079053 (to R.G. Tilton); by the James W. McLaughlin Fellowship Fund (to B.C. Tieu); by National Institute of Environmental Health Sciences (NIEHS) Predoctoral Fellowship T32ES007254 (to B.C. Tieu); by NIEHS, NIH, grant P30 ES06676 (to J. Halpert, University of Texas Medical Branch); and by NIH grant BAA-HL-02-04 (to A. Kurosky, University of Texas Medical Branch).

Received for publication December 11, 2008, and accepted in revised form September 23, 2009.

Address correspondence to: Allan R. Brasier, MRB 8.128, 301 University Blvd., Galveston, Texas 77555-1060, USA. Phone: (409) 772-2824; Fax: (409) 772-8709; E-mail: arbrasie@utmb.edu.

1. Beckman, J.A. 2006. Aortic aneurysms: pathophysiology, epidemiology, and prognosis. In *Vascular medicine*. M.A. Creager, V.J. Dzau, and J. Loscalzo, editors. W.B. Saunders/Elsevier. Philadelphia, Pennsylvania, USA. 543–559.
2. Kuivaniemi, H., Platsoucas, C.D., and Tilson, M.D., 3rd. 2008. Aortic aneurysms: an immune disease with a strong genetic component. *Circulation*. **117**:242–252.
3. Guo, D.C., Papke, C.L., He, R., and Milewicz, D.M. 2006. Pathogenesis of thoracic and abdominal aortic aneurysms. *Ann. N. Y. Acad. Sci.* **1085**:339–352.
4. He, R., et al. 2006. Characterization of the inflammatory and apoptotic cells in the aortas of patients with ascending thoracic aortic aneurysms and dissections. *J. Thorac. Cardiovasc. Surg.* **131**:671–678.
5. Daugherty, A., and Cassis, L.A. 2002. Mechanisms of abdominal aortic aneurysm formation. *Curr. Atheroscler. Rep.* **4**:222–227.
6. Shimizu, K., Mitchell, R.N., and Libby, P. 2006. Inflammation and cellular immune responses in abdominal aortic aneurysms. *Arterioscler. Thromb. Vasc. Biol.* **26**:987–994.
7. Shah, P.K. 1997. Inflammation, metalloproteinases, and increased proteolysis: an emerging pathophysiological paradigm in aortic aneurysm. *Circulation*. **96**:2115–2117.
8. Ross, R. 1999. Atherosclerosis — an inflammatory disease. *N. Engl. J. Med.* **340**:115–126.
9. MacTaggart, J.N., Xiong, W., Knispel, R., and Baxter, B.T. 2007. Deletion of CCR2 but not CCR5 or CXCR3 inhibits aortic aneurysm formation. *Surgery*. **142**:284–288.
10. Ishibashi, M., et al. 2004. Bone marrow-derived monocyte chemoattractant protein-1 receptor CCR2 is critical in angiotensin II-induced acceleration of atherosclerosis and aneurysm formation in hypercholesterolemic mice. *Arterioscler. Thromb. Vasc. Biol.* **24**:e174–e178.
11. Ishibashi, M., et al. 2004. Critical role of monocyte chemoattractant protein-1 receptor CCR2 on monocytes in hypertension-induced vascular inflammation and remodeling. *Circ. Res.* **94**:1203–1210.
12. Bush, E., et al. 2000. CC chemokine receptor 2 is required for macrophage infiltration and vascular hypertrophy in angiotensin II-induced hypertension. *Hypertension*. **36**:360–363.
13. Jones, K.G., et al. 2001. Interleukin-6 (IL-6) and the prognosis of abdominal aortic aneurysms. *Circulation*. **103**:2260–2265.
14. Cheuk, B.L., and Cheng, S.W. 2008. Can local secretion of prostaglandin E2, thromboxane B2, and interleukin-6 play a role in ruptured abdominal aortic aneurysm? *World J. Surg.* **32**:55–61.
15. Dawson, J., et al. 2007. Aortic aneurysms secrete interleukin-6 into the circulation. *J. Vasc. Surg.* **45**:350–356.
16. Dawson, J., Cockerill, G., Choke, E., Loftus, I., and Thompson, M.M. 2006. Aortic aneurysms as a source of circulating interleukin-6. *Ann. N. Y. Acad. Sci.* **1085**:320–323.
17. Juvonen, J., et al. 1997. Elevated circulating levels of inflammatory cytokines in patients with abdominal aortic aneurysm. *Arterioscler. Thromb. Vasc. Biol.* **17**:2843–2847.
18. Szekanecz, Z., Shah, M.R., Pearce, W.H., and Koch, A.E. 1994. Human atherosclerotic abdominal aortic aneurysms produce interleukin (IL)-6 and interferon-gamma but not IL-2 and IL-4: the possible role for IL-6 and interferon-gamma in vascular inflammation. *Agents Actions*. **42**:159–162.
19. Treska, V., Topolcan, O., and Pecen, L. 2000. Cytokines as plasma markers of abdominal aortic aneurysm. *Clin. Chem. Lab. Med.* **38**:1161–1164.
20. Rohde, L.E., et al. 1999. Plasma concentrations of interleukin-6 and abdominal aortic diameter among subjects without aortic dilatation. *Arterioscler. Thromb. Vasc. Biol.* **19**:1695–1699.
21. Ikeda, U., Ito, T., and Shimada, K. 2001. Interleukin-6 and acute coronary syndrome. *Clin. Cardiol.* **24**:701–704.
22. Schieffer, B., et al. 2000. Expression of angiotensin II and interleukin 6 in human coronary atherosclerotic plaques: potential implications for inflammation and plaque instability. *Circulation*. **101**:1372–1378.
23. Biasucci, L.M., et al. 1999. Increasing levels of interleukin (IL)-1Ra and IL-6 during the first 2 days of hospitalization in unstable angina are associated with increased risk of in-hospital coronary events. *Circulation*. **99**:2079–2084.
24. Tieying, H., et al. 2008. Roles of IL-6-gp130 signaling in vascular inflammation. *Curr. Cardiol. Rev.* **4**:179–192.
25. Brasier, A.R., Recinos, A., 3rd, and Eledrisi, M.S. 2002. Vascular inflammation and the renin-angiotensin system. *Arterioscler. Thromb. Vasc. Biol.* **22**:1257–1266.
26. Michel, J.B., et al. 2007. Topological determinants and consequences of adventitial responses to arterial wall injury. *Arterioscler. Thromb. Vasc. Biol.* **27**:1259–1268.
27. Koch, A.E., et al. 1990. Human abdominal aortic aneurysms. Immunophenotypic analysis suggesting an immune-mediated response. *Am. J. Pathol.* **137**:1199–1213.
28. Sakata, N., et al. 2007. Possible involvement of myofibroblasts in the development of inflammatory aortic aneurysm. *Pathol. Res. Pract.* **203**:21–29.
29. Recinos, A., 3rd, et al. 2007. Angiotensin II induces IL-6 expression and the Jak-STAT3 pathway in aortic adventitia of LDL receptor-deficient mice. *Atherosclerosis*. **194**:125–133.
30. Ramshaw, A.L., Roskell, D.E., and Parums, D.V. 1994. Cytokine gene expression in aortic adventitial inflammation associated with advanced atherosclerosis (chronic periaortitis). *J. Clin. Pathol.* **47**:721–727.
31. Maiellaro, K., and Taylor, W.R. 2007. The role of the adventitia in vascular inflammation. *Cardiovasc. Res.* **75**:640–648.
32. Moreno, P.R., Purushothaman, K.R., Fuster, V., and O'Connor, W.N. 2002. Intimomedial interface damage and adventitial inflammation is increased beneath disrupted atherosclerosis in the aorta: implications for plaque vulnerability. *Circulation*. **105**:2504–2511.
33. Schwartz, C.J., and Mitchell, J.R. 1962. Cellular infiltration of the human arterial adventitia associated with atheromatous plaques. *Circulation*. **26**:73–78.
34. Longo, G.M., et al. 2002. Matrix metalloproteinases 2 and 9 work in concert to produce aortic aneurysms. *J. Clin. Invest.* **110**:625–632.
35. Freestone, T., et al. 1995. Inflammation and matrix metalloproteinases in the enlarging abdominal aortic aneurysm. *Arterioscler. Thromb. Vasc. Biol.* **15**:1145–1151.
36. Cui, R., Tieu, B., Recinos, A., Tilton, R.G., and Brasier, A.R. 2006. RhoA mediates angiotensin II-induced phospho-Ser536 nuclear factor kappaB/RelA subunit exchange on the interleukin-6 promoter in VSMCs. *Circ. Res.* **99**:723–730.
37. Daugherty, A., Manning, M.W., and Cassis, L.A. 2000. Angiotensin II promotes atherosclerotic lesions and aneurysms in apolipoprotein E-deficient mice. *J. Clin. Invest.* **105**:1605–1612.
38. Daugherty, A., and Cassis, L. 1999. Chronic angiotensin II infusion promotes atherogenesis in low density lipoprotein receptor –/– mice. *Ann. N. Y. Acad. Sci.* **892**:108–118.

39. Deng, G., et al. 2003. Urokinase-type plasminogen activator plays a critical role in angiotensin II-induced abdominal aortic aneurysm. *Circ. Res.* **92**:510–517.
40. Wang, Y.X., et al. 2001. Angiotensin II increases urokinase-type plasminogen activator expression and induces aneurysm in the abdominal aorta of apolipoprotein E-deficient mice. *Am. J. Pathol.* **159**:1455–1464.
41. Rogers, H.W., and Unanue, E.R. 1993. Neutrophils are involved in acute, nonspecific resistance to Listeria monocytogenes in mice. *Infect. Immun.* **61**:5090–5096.
42. Ezekowitz, R.A., and Gordon, S. 1982. Down-regulation of mannosyl receptor-mediated endocytosis and antigen F4/80 in bacillus Calmette-Guerin-activated mouse macrophages. Role of T lymphocytes and lymphokines. *J. Exp. Med.* **155**:1623–1637.
43. Ezekowitz, R.A., Austyn, J., Stahl, P.D., and Gordon, S. 1981. Surface properties of bacillus Calmette-Guerin-activated mouse macrophages. Reduced expression of mannose-specific endocytosis, Fc receptors, and antigen F4/80 accompanies induction of Ia. *J. Exp. Med.* **154**:60–76.
44. Chomarat, P., Banchereau, J., Davoust, J., and Palucka, A.K. 2000. IL-6 switches the differentiation of monocytes from dendritic cells to macrophages. *Nat. Immunol.* **1**:510–514.
45. Liu, E., Tu, W., Law, H.K., and Lau, Y.L. 2001. Changes of CD14 and CD1a expression in response to IL-4 and granulocyte-macrophage colony-stimulating factor are different in cord blood and adult blood monocytes. *Pediatr. Res.* **50**:184–189.
46. Weiss, D., Kools, J.J., and Taylor, W.R. 2001. Angiotensin II-induced hypertension accelerates the development of atherosclerosis in apoE-deficient mice. *Circulation.* **103**:448–454.
47. Lu, H., Rateri, D.L., Cassis, L.A., and Daugherty, A. 2008. The role of the renin-angiotensin system in aortic aneurysmal diseases. *Curr. Hypertens. Rep.* **10**:99–106.
48. Golledge, J., Muller, J., Daugherty, A., and Norman, P. 2006. Abdominal aortic aneurysm: pathogenesis and implications for management. *Arterioscler. Thromb. Vasc. Biol.* **26**:2605–2613.
49. Daugherty, A., and Cassis, L. 2004. Angiotensin II and abdominal aortic aneurysms. *Curr. Hypertens. Rep.* **6**:442–446.
50. Saraff, K., Babamusta, F., Cassis, L.A., and Daugherty, A. 2003. Aortic dissection precedes formation of aneurysms and atherosclerosis in angiotensin II-infused, apolipoprotein E-deficient mice. *Arterioscler. Thromb. Vasc. Biol.* **23**:1621–1626.
51. Swirski, F.K., et al. 2007. Ly-6Chi monocytes dominate hypercholesterolemia-associated monocytosis and give rise to macrophages in atheromata. *J. Clin. Invest.* **117**:195–205.
52. Moos, M.P., et al. 2005. The lamina adventitia is the major site of immune cell accumulation in standard chow-fed apolipoprotein E-deficient mice. *Arterioscler. Thromb. Vasc. Biol.* **25**:2386–2391.
53. Sun, J., et al. 2007. Mast cells modulate the pathogenesis of elastase-induced abdominal aortic aneurysms in mice. *J. Clin. Invest.* **117**:3359–3368.
54. Capers, Q., et al. 1997. Monocyte chemoattractant protein-1 expression in aortic tissues of hypertensive rats. *Hypertension.* **30**:1397–1402.
55. Rayner, K., Van, E.S., Groot, P.H., and Reape, T.J. 2000. Localisation of mRNA for JE/MCP-1 and its receptor CCR2 in atherosclerotic lesions of the ApoE knockout mouse. *J. Vasc. Res.* **37**:93–102.
56. Forester, N.D., Cruickshank, S.M., Scott, D.J., and Carding, S.R. 2005. Functional characterization of T cells in abdominal aortic aneurysms. *Immunology.* **115**:262–270.
57. Herron, G.S., et al. 1991. Connective tissue proteinases and inhibitors in abdominal aortic aneurysms. Involvement of the vasa vasorum in the pathogenesis of aortic aneurysms. *Arterioscler. Thromb.* **11**:1667–1677.
58. Miyata, K., et al. 2000. Rho-kinase is involved in macrophage-mediated formation of coronary vascular lesions in pigs in vivo. *Arterioscler. Thromb. Vasc. Biol.* **20**:2351–2358.
59. Rogers, C., Edelman, E.R., and Simon, D.I. 1998. A mAb to the beta2-leukocyte integrin Mac-1 (CD11b/CD18) reduces intimal thickening after angioplasty or stent implantation in rabbits. *Proc. Natl. Acad. Sci. U. S. A.* **95**:10134–10139.
60. Ross, G.D. 2002. Role of the lectin domain of Mac-1/CR3 (CD11b/CD18) in regulating intercellular adhesion. *Immunol. Res.* **25**:219–227.
61. Shi, C., et al. 2004. Integrin engagement regulates monocyte differentiation through the forkhead transcription factor Foxp1. *J. Clin. Invest.* **114**:408–418.
62. Romano, M., et al. 1997. Role of IL-6 and its soluble receptor in induction of chemokines and leukocyte recruitment. *Immunity.* **6**:315–325.
63. Yang, X.P., et al. 2005. Signal transducer and activator of transcription 3alpha and specificity protein 1 interact to upregulate intercellular adhesion molecule-1 in ischemic-reperfused myocardium and vascular endothelium. *Arterioscler. Thromb. Vasc. Biol.* **25**:1395–1400.
64. Noda-Heiny, H., Daugherty, A., and Sobel, B.E. 1995. Augmented urokinase receptor expression in atheroma. *Arterioscler. Thromb. Vasc. Biol.* **15**:37–43.
65. Xue, W., Kindzelskii, A.L., Todd, R.F., 3rd, and Petty, H.R. 1994. Physical association of complement receptor type 3 and urokinase-type plasminogen activator receptor in neutrophil membranes. *J. Immunol.* **152**:4630–4640.
66. Wong, W.S., Simon, D.I., Rosoff, P.M., Rao, N.K., and Chapman, H.A. 1996. Mechanisms of pertussis toxin-induced myelomonocytic cell adhesion: role of Mac-1(CD11b/CD18) and urokinase receptor (CD87). *Immunology.* **88**:90–97.
67. Sitrin, R.G., Todd, R.F., 3rd, Albrecht, E., and Gyetko, M.R. 1996. The urokinase receptor (CD87) facilitates CD11b/CD18-mediated adhesion of human monocytes. *J. Clin. Invest.* **97**:1942–1951.
68. Gyetko, M.R., Todd, R.F., 3rd, Wilkinson, C.C., and Sitrin, R.G. 1994. The urokinase receptor is required for human monocyte chemotaxis in vitro. *J. Clin. Invest.* **93**:1380–1387.
69. Simon, D.I., et al. 1996. Mac-1 (CD11b/CD18) and the urokinase receptor (CD87) form a functional unit on monocytic cells. *Blood.* **88**:3185–3194.
70. Pluskota, E., Soloviev, D.A., and Plow, E.F. 2003. Convergence of the adhesive and fibrinolytic systems: recognition of urokinase by integrin alpha Mbeta 2 as well as by the urokinase receptor regulates cell adhesion and migration. *Blood.* **101**:1582–1590.
71. Gong, Y., Hart, E., Shchurin, A., and Hoover-Plow, J. 2008. Inflammatory macrophage migration requires MMP-9 activation by plasminogen in mice. *J. Clin. Invest.* **118**:3012–3024.
72. Simpson, P.J., et al. 1988. Reduction of experimental canine myocardial reperfusion injury by a monoclonal antibody (anti-Mo1, anti-CD11b) that inhibits leukocyte adhesion. *J. Clin. Invest.* **81**:624–629.
73. Daugherty, A., and Cassis, L. 2004. Angiotensin II-mediated development of vascular diseases. *Trends Cardiovasc. Med.* **14**:117–120.
74. Babamusta, F., et al. 2006. Angiotensin II infusion induces site-specific intra-laminar hemorrhage in macrophage colony-stimulating factor-deficient mice. *Atherosclerosis.* **186**:282–290.
75. Moulton, K.S., et al. 2003. Inhibition of plaque neovascularization reduces macrophage accumulation and progression of advanced atherosclerosis. *Proc. Natl. Acad. Sci. U. S. A.* **100**:4736–4741.